*Wind and Structures, Vol. 6, No. 1 (2003) 1-22*
DOI: http://dx.doi.org/10.12989/was.2003.6.1.001


# 3-D wind-induced effects on bridges during balanced cantilever erection stages

Stefan Schmidt†

*Parsons*

Giovanni Solari‡

*Department of Structural and Geotechnical Engineering, University of Genoa, Italy*
*(Received Fubruary 16, 2002, Accepted October 3, 2002)*

**Abstract.** Nowadays balanced cantilever construction plays an essential role as a sophisticated erection technique of bridges due to its economical and ecological advantages. Experience teaches that wind has a great importance with regard to this construction technique, but methods proposed by codes to take wind effects into account are still rather crude and, in most cases, completely lacking. Also research in this field is quite limited and aimed at studying only the longitudinal shear and the torque at the pier base, caused by the mean wind velocity and by the longitudinal turbulence actions over the deck. This paper advances the present solutions by developing a new procedure that takes into account all wind effects both on the deck and on the pier. The proposed model assumes the mean wind velocity as orthogonal to the bridge plane and considers the effects produced by all the three turbulence components and by the vortex shedding. The applications point out the role of each loading component on different bridge configurations and show that disregarding the presence of some effects may imply oversimplified results and relevant underestimations.

**Key words:** alongwind vibrations; atmospheric turbulence; bridges; cantilever erection stages; crosswind vibrations; maximum response; torsional vibrations; vortex shedding; wind engineering; 3D wind-induced effects.

## 1. Introduction

Balanced cantilever construction of bridges arose from a need to overcome construction difficulties in spanning deep valleys and river crossing without the use of conventional falsework, which may be impractical, economically prohibitive, or detrimental to environment and ecology. Cantilever construction, whether cast-in-place or pre-cast, eliminates such difficulties since erection proceeds from the piers and the structure is self-supporting at all its stages. From first applications in the 50's, until today, this technique has been developed rapidly and more and more major projects using balanced cantilever erection are being built all over the world.

Experience teaches that wind has a great importance with regard to this construction technique,

† Formerly, Bauhaus, University Weimar, Germany
‡ Professor

whereby its role is more critical when the wind climate at the site is severe or the structure is sensitive to dynamic wind actions due to tall and flimsy piers or long cantilever arms. However, despite this attribute, the methods proposed by codes to take wind effects into account during balanced cantilever erection stages are still rather crude (AASHTO 1996). In addition, research in this field is quite limited (Dyrbye and Hansen 1997, Mendes and Branco 2001) and aimed at studying only the longitudinal shear force and the torsional moment induced by the mean wind velocity and by the longitudinal turbulence over the deck, completely ignoring wind actions on pier and, even more, the role of the lateral and vertical turbulence components and of the vortex shedding.

Starting from above premises, a complete model of the pier and of the cantilever arms has been formulated, including the variable curvature of the bridge deck and all other typical structural properties in order to suit actual engineering solutions and guarantee a broad band of application in the construction sector. The model is subjected to the mean wind velocity, assumed orthogonal to the bridge plane, to the three spatial components of the atmospheric turbulence and to the vortex shedding (Schmidt 2001). It furnishes the statistical parameters of the six internal forces (the axial force, two shear forces, two bending moments and the torque) along the pier, each expressed as the sum of its static, quasi-static and resonant parts. The static and the quasi-static parts are determined by the influence function technique (Kasperski 1992, Holmes 1994, Davenport 1995). The resonant part is calculated by taking all dominant vibration modes into account (Solari 1989, Davenport 1995, Holmes 2002). Analyses are carried out in the frequency domain by the classic methods of process theory and random dynamics. Due to such properties, the proposed method generalises the model developed by the second author and his research group from cantilever vertical structures (Piccardo and Solari 1998, 2000, 2002) to bridges during balanced cantilever erection stages. It also completes and extends the approaches formulated in Dyrbye and Hansen (1997), Mendes and Branco (2001).

The model was applied to examine three realised bridge projects in balanced cantilever erection stages (Schmidt 2001), whereby only an extract of two examples is reproduced here for the sake of space. Comparisons with results provided by AASHTO provisions (AASHTO 1996) and by previous contributions to this field (Dyrbye and Hansen 1997, Mendes and Branco 2001) point out the role of the different wind loading components on different bridge configurations. They also show that disregarding the presence of some effects may imply oversimplified results and relevant underestimations. The conclusions discuss the progress and the prospects involved by the proposed model but, in the meanwhile, the necessity of checking and calibrating it through wind tunnel tests and full-scale experiments.

## 2. Structural geometry and wind loading model

Let us consider a Cartesian reference system with origin at $O$ on the soil; $z$ coincides with the pier axis; $y$ is parallel to the deck axis, $x$ is perpendicular to the bridge plane. Fig. 1 shows the structural geometry, where $H_p$ is the height of the pier, $H_d$ is the height of the deck centre, $R$ and $L$ are the lengths of the right and left cantilever arms, respectively, $b_p$ and $b_d$ are reference widths of the pier and of the deck, respectively. The structure is assumed as statically determined due to a fixed restraint at the base of the pier and to a rigid connection between the deck and the pier.

The bridge is immersed in a wind field whose mean wind velocity $\overline{u}$ is aligned with $x$ (Fig. 2); $u'$, $v'$ and $w'$ are the longitudinal ($x$), lateral ($y$) and vertical ($z$) turbulent fluctuations treated here as

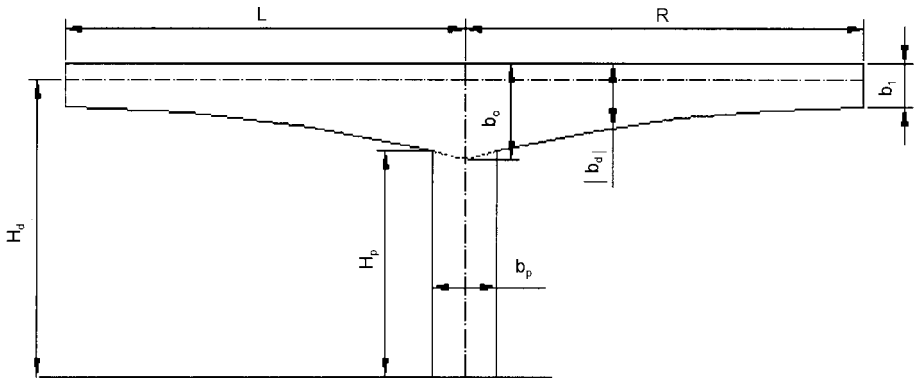


Fig. 1 Structural geometry

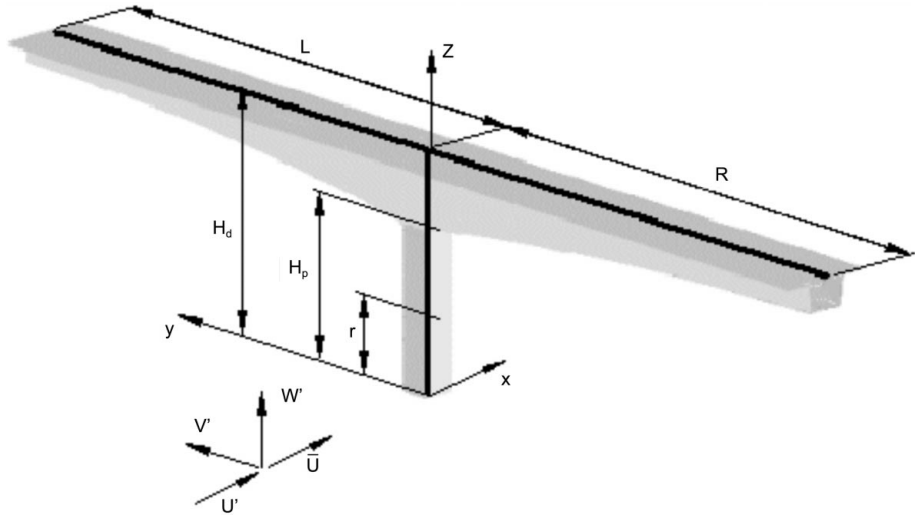


Fig. 2 Structural scheme and reference system

stochastic stationary Gaussian independent processes. Furthermore $u'/\bar{u} << 1$, $v'/\bar{u} << 1$ and $w'/\bar{u} << 1$.

Coherently with the wind loading model proposed in Piccardo and Solari (2000), the aerodynamic actions on the pier ($F_p$) and on the deck ($F_d$) are defined as:

$$F_{p\kappa}(z;t) = \bar{F}_{p\kappa}(z) + F'_{p\kappa}(z;t) \tag{1}$$

$$F_{d\kappa}(y;t) = \bar{F}_{d\kappa}(y) + F'_{d\kappa}(y;t) \tag{2}$$

where $t$ is the time; $0 \le z \le H_p$; $-R \le y \le L$; $\kappa = 1,2,3$ correspond to the forces along $x$, $y$, $z$ and $\kappa = 4, 5, 6$ correspond to the moments around $x$, $y$, $z$; $\bar{F}_{p\kappa}$ and $\bar{F}_{d\kappa}$ are the mean values of $F_{p\kappa}$ and $F_{d\kappa}$, respectively; $F'_{p\kappa}$ and $F'_{d\kappa}$ are, respectively, the nil mean fluctuations of $F_{p\kappa}$ and $F_{d\kappa}$ around $\bar{F}_{p\kappa}$

and $\bar{F}_{d\kappa}$. They are defined as:

$$\bar{F}_{p\kappa}(z) = \frac{1}{2}\rho\bar{u}^2(z)b_p\lambda_{p\kappa}c_{p\kappa u}\gamma_{p\kappa u}(z) \tag{3a}$$

$$\bar{F}_{d\kappa}(y) = \frac{1}{2}\rho\bar{u}^2(H_d)b_d\lambda_{d\kappa}c_{d\kappa u}\gamma_{d\kappa u}(y) \tag{3b}$$

$$F'_{p\kappa}(z;t) = \sum\nolimits_{\varepsilon} F'_{p\kappa\varepsilon}(z;t);\ \ F'_{p\kappa\varepsilon}(z;t) = \frac{1}{2}\rho\bar{u}^2(z)b_p\lambda_{p\kappa}c_{p\kappa\varepsilon}\gamma_{p\kappa\varepsilon}(z)J_{\varepsilon}(z)f^*_{p\kappa\varepsilon}(z;t) \tag{4a}$$

$$F'_{d\kappa}(z;t) = \sum\nolimits_{\varepsilon} F'_{d\kappa\varepsilon}(y;t);\ \ F'_{d\kappa\varepsilon}(y;t) = \frac{1}{2}\rho\bar{u}^2(H_d)b_d\lambda_{d\kappa}c_{d\kappa\varepsilon}\gamma_{d\kappa\varepsilon}(y)J_{\varepsilon}(H_d)f^*_{d\kappa\varepsilon}(y;t) \tag{4b}$$

where $\rho$ is the air density; $\lambda_{pk}$ and $\lambda_{dk}$ are the $\kappa$-th components of the vectors $\{\lambda_p\} = \{1\ 1\ 1\ b_p\ b_p\ b_p\}^T$ and $\{\lambda_p\} = \{1\ 1\ 1\ b_d\ b_d\ b_d\}^T$, respectively; $\Sigma_\varepsilon$ is the sum of four loading terms with indices $\varepsilon = u, v, w, s$, associated with the three turbulence components ($u'$, $v'$ and $w'$) and with the wake excitation ($s'$); $c_{p\kappa\varepsilon}$ and $c_{d\kappa\varepsilon}$ are the $\kappa,\varepsilon$-th elements of the aerodynamic matrixes of the pier and of the deck, respectively:

$$[c_p] = \begin{bmatrix} c_{dp} & 0 & 0 & 0 \\ 0 & c_{dp}+c'_{lp} & 0 & \tilde{c}_{lsp} \\ 0 & 0 & 0 & 0 \\ 0 & 0 & 0 & 0 \\ 0 & 0 & 0 & 0 \\ 0 & c'_{mp} & 0 & \tilde{c}_{msp} \end{bmatrix};\ [c_d] = \begin{bmatrix} c_{dd} & 0 & c'_{dd}-c_{ld} & 0 \\ 0 & 0 & 0 & 0 \\ c_{ld} & 0 & c_{dd}+c'_{ld} & \tilde{c}_{lsd} \\ 0 & 0 & 0 & 0 \\ c_{md} & 0 & c'_{md} & \tilde{c}_{msd} \\ 0 & 0 & 0 & 0 \end{bmatrix} \tag{5}$$

where $c_{dp}$, $c_{lp}$, $c_{mp}$ and $c_{dd}$, $c_{ld}$, $c_{md}$ are the drag, lift and torsional moment coefficients for the pier and for the deck, respectively; $c'_{dp}$, $c'_{lp}$, $c'_{mp}$ and $c'_{dd}$, $c'_{ld}$, $c'_{md}$ are the angular derivates of $c_{dp}$, $c_{lp}$, $c_{mp}$ and of $c_{dd}$, $c_{ld}$, $c_{md}$, respectively; $\tilde{c}_{dsp}$, $\tilde{c}_{lsp}$, $\tilde{c}_{msp}$ and $\tilde{c}_{dsd}$, $\tilde{c}_{lsd}$, $\tilde{c}_{msd}$ are the root mean square (rms) values of the drag, lift and torsional moment wake coefficients for the pier and for the deck, respectively, whereby $\tilde{c}_{dsp} = \tilde{c}_{dsd} = 0$; $J_u = 2I_u$, $J_v = I_v$, $J_w = I_w$, $J_s = 1$, where $I_u = \sigma_u/\bar{u}$, $I_v = \sigma_v/\bar{u}$, $I_w = \sigma_w/\bar{u}$ are the turbulence intensities, $\sigma_u$, $\sigma_v$, $\sigma_w$ are the rms values of $u'$, $v'$, $w'$; $f^*_{p\kappa\varepsilon}$ and $f^*_{d\kappa\varepsilon}$ are the $\varepsilon$-th component of the row vectors:

$$\{f^*_{p\kappa}(z;t)\} = \{u^*(0,z;t)\ \ v^*(0,z;t)\ \ w^*(0,z;t)\ \ s^*_{p\kappa}(z;t)\} \tag{6a}$$

$$\{f^*_{d\kappa}(y;t)\} = \{u^*(y,H_d;t)\ \ v^*(y,H_d;t)\ \ w^*(y,H_d;t)\ \ s^*_{d\kappa}(z;t)\} \tag{6b}$$

where $u^* = u'/\sigma_u$, $v^* = v'/\sigma_v$, $w^* = w'/\sigma_w$ are the reduced turbulence components; $s^*_{p\kappa}$ and $s^*_{d\kappa}$ are the $\kappa$-th reduced components of the wake excitation of the pier and of the deck, respectively, treated as stochastic stationary Gaussian processes independent of $u^*$, $v^*$ and $w^*$ (Solari 1985); $\gamma_{p\kappa\varepsilon}$ and $\gamma_{d\kappa\varepsilon}$ are nondimensional shape functions that make the model suitable for variable properties of the pier and of the deck, respectively.

The cross-power spectral density function (cpsdf) of the atmospheric turbulence is expressed as:

$$S^*_{\varepsilon}(M,M';n) = \sqrt{S^*_{\varepsilon}(z;n)S^*_{\varepsilon}(z';n)}\,\mathrm{coh}_{\varepsilon}(M,M';n) \quad (\varepsilon = u', v', w') \tag{7}$$

where $n$ is the frequency; $M$ is a point of coordinates $y$, $z$; $M'$ is a point of coordinates $y'$, $z'$; $S_{\varepsilon}^{*}(z;n)$ is the psdf of $\varepsilon^{*}(M;t)$; $\mathrm{coh}_{\varepsilon}(M, M';n)$ is the coherence function of $\varepsilon^{*}(M;t)$ and $\varepsilon^{*}(M';t)$.

The analyses developed here are based on the following spectral equations (Solari and Piccardo 2001):

$$S_{\varepsilon}^{*}(z;n) = \frac{d_{\varepsilon} n L_{\varepsilon}(z)/\bar{u}(z)}{[1 + 1.5 d_{\varepsilon} n L_{\varepsilon}(z)/\bar{u}(z)]^{5/3}} \quad (\varepsilon = u', v', w') \tag{8}$$

$$\mathrm{coh}_{\varepsilon}(M, M';n) = \exp\left\{-\frac{2n\sqrt{C_{y\varepsilon}^{2}|y-y'|^{2} + C_{z\varepsilon}^{2}|z-z'|^{2}}}{\bar{u}(z) + \bar{u}(z')}\right\} \quad (\varepsilon = u', v', w') \tag{9}$$

where $d_u = 6.868$, $d_v = d_w = 9.434$; $L_{\varepsilon}$ is the integral length scale of the $\varepsilon$ turbulence component in $x$-direction; $C_{y\varepsilon}$ and $C_{z\varepsilon}$ are the exponential decay coefficients of the $\varepsilon$ turbulence component along $y$ and $z$, respectively. Fig. 3 shows the particularisation of Eq. (9) to the analysed structure.

The cpsdf of the wake excitation is expressed as:

$$S_{s}^{*}(M, M';n) = \sqrt{S_{q\kappa}^{*}(z;n) S_{q\kappa}^{*}(z';n)}\,\mathrm{coh}_{q}(r, r';n) \tag{10}$$

where $M$ and $M'$ are points belonging both to the pier or to the deck. If $M$ and $M'$ belong to the pier, $q = p$ and $r = z$; if $M$ and $M'$ belong to the deck, $q = d$ and $r = y$. $S_{p\kappa}^{*}(z;n)$ and $S_{d\kappa}^{*}(y;n)$ are the psdf of the wake excitation of the pier and of the deck, respectively; $\mathrm{coh}_{q}(r, r';n)$ is the two-point coherence function. They are given by the relationships (Vickery and Clark 1972, Engineering Sciences Data Unit 1990):

$$S_{q\kappa}^{*}(r;n) = \frac{1}{\sqrt{\pi} B_{q\kappa}(r) n_{q\kappa}(r)} \exp\left\{-\left[\frac{1 - n/n_{q\kappa}(r)}{B_{q\kappa}(r)}\right]^{2}\right\} \tag{11}$$

$$\mathrm{coh}_{q}(r, r';n) = \exp\left\{-\frac{|r-r'|}{\mathcal{L}_{q} b_{q}}\right\} \tag{12}$$

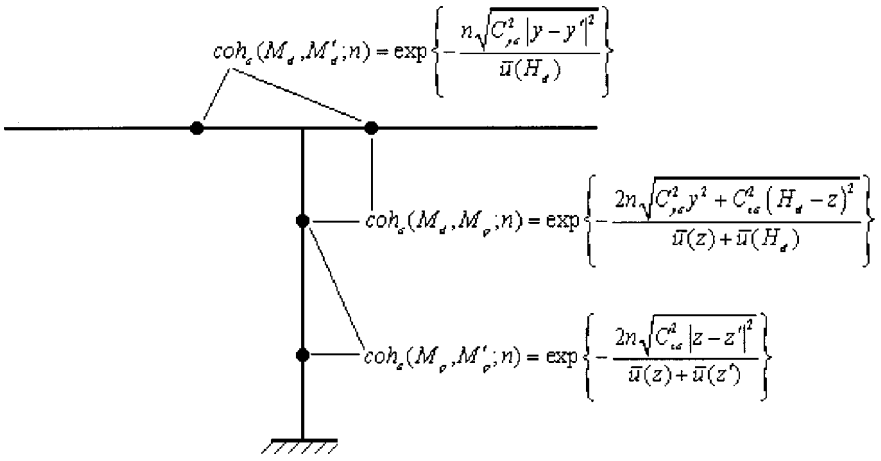


Fig. 3 Two-point coherence function ($\varepsilon = u', v', w'$)

where $n_{q\kappa}(r) = Y_{q\kappa} S_q \bar{u}(r)/b_q(r)$ is the shedding frequency; $b_p(z)$ and $b_d(y)$ are the current widths of the pier and of the deck, respectively; $S_p$ and $S_d$ are the Strouhal numbers of the pier and of the deck, respectively; $Y_{p\kappa}$ and $Y_{d\kappa}$ are the $\kappa$-th components of the vectors $\{Y_p\}=\{2\ 1\ 0\ 0\ 0\ Y_{p\theta}\}^T$ and $\{Y_d\}=\{2\ 0\ 1\ 0\ Y_{d\theta}\ 0\}^T$, respectively, where $Y_{p\theta}$ and $Y_{d\theta}$ are appropriate shape factors (Solari 1985); $B_{q\kappa}(r)$ is the bandwidth spectral parameter; $\mathcal{L}_q$ is the correlation length (in $b_q$'s) of the vortex shedding. It is assumed that the wake excitation of the pier and of the deck constitute independent random processes.

## 3. Wind-induced effects

Wind-induced effects on the cantilever arms of the deck may be determined easily by generalising the model proposed in Piccardo and Solari (2002) from vertical to horizontal structures. However, the most important effects for the bridge stability during erection are those induced by wind along the pier and, especially, the internal forces at the pier base. Let us define by $E_i(r)$ the $i$-th component of the internal force at height $r$ along the pier (Fig. 2), where $E_1$ is the shear force in $x$-direction; $E_2$ is the shear force in $y$-direction; $E_3$ is the normal force in $z$-direction; $E_4$ is the bending moment around the $x$-axis; $E_5$ is the bending moment around the $y$-axis; $E_6$ is the torque around the $z$-axis (Fig. 4). These quantities are expressed as:

$$E_i(r;t) = \bar{E}_i(r) + E_i'(r;t) \ ; \ E_i'(r;t) = E_{Qi}'(r;t) + E_{Di}'(r;t) \tag{13}$$

where $\bar{E}_i(r)$ is the mean static effect and $E_i'(r;t)$ is the zero mean fluctuating effect, splitted herein in two parts, namely the quasi-static part $E_{Qi}'(r;t)$ and the resonant part $E_{Di}'(r;t)$.

Using the influence function technique, the mean static effect and the quasi-static part of the effect are given by:

$$\bar{E}_i(r) = \sum_{\kappa=1}^{6} \bar{E}_{i\kappa}(r) \ ; \ \bar{E}_{i\kappa}(r) = \int_0^{Hp} \bar{F}_{p\kappa}(z)\,\eta_{pi\kappa}(z,r)\,dz + \int_{-R}^{L} \bar{F}_{d\kappa}(y)\,\eta_{di\kappa}(y,r)\,dy \tag{14}$$

$$E_{Qi}'(r;t) = \sum_{\kappa=1}^{6} E_{Qi\kappa}'(r;t) \ ; \ E_{Qi\kappa}'(r;t) = \int_0^{Hp} F_{p\kappa}'(z;t)\,\eta_{pi\kappa}(z,r)\,dz + \int_{-R}^{L} F_{d\kappa}'(y;t)\,\eta_{di\kappa}(y,r)\,dy \tag{15}$$

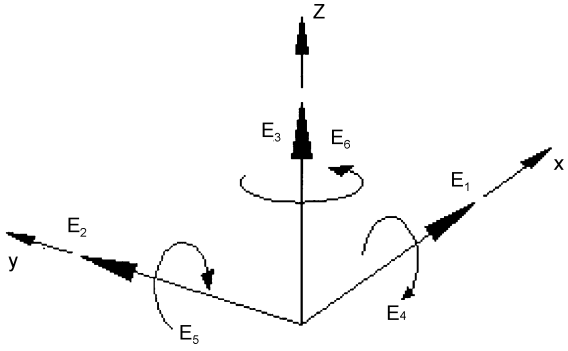


Fig. 4 Internal forces along the pier

where $\bar{E}_{i\kappa}(r)$ and $E'_{Qi\kappa}(r;t)$ are, respectively, the contributions to $\bar{E}_i(r)$ and to $E'_{Qi}(r;t)$ due to the $\kappa$-th loading component; $\eta_{pi\kappa}(z,r)$ is the influence function for the pier, i.e., the $i$-th internal force at height $r$ of the pier due to a unit static action $F_{p\kappa}$ at the height $z$ of the pier; $\eta_{di\kappa}(y,r)$ is the influence function for the deck, i.e. the $i$-th internal force at height $r$ of the pier due to a unit static action $F_{d\kappa}$ at a point of the deck with coordinate $y$. They represent the $\kappa,i$-th terms of the following matrixes:

$$[\eta_p(z,r)] = \begin{bmatrix} \Phi(z-r) & 0 & 0 & 0 & 0 & 0 \\ 0 & \Phi(z-r) & 0 & 0 & 0 & 0 \\ 0 & 0 & \Phi(z-r) & 0 & 0 & 0 \\ 0 & -(z-r)\Phi(z-r) & 0 & 0 & 0 & 0 \\ (z-r)\Phi(z-r) & 0 & 0 & 0 & 0 & 0 \\ 0 & 0 & 0 & 0 & 0 & \Phi(z-r) \end{bmatrix} \tag{16a}$$

$$[\eta_d(y,r)] = \begin{bmatrix} 1 & 0 & 0 & 0 & 0 & 0 \\ 0 & 1 & 0 & 0 & 0 & 0 \\ 0 & 0 & 1 & 0 & 0 & 0 \\ 0 & -(H_d-r) & y & 0 & 0 & 0 \\ H_d-r & 0 & 0 & 0 & 1 & 0 \\ -y & 0 & 0 & 0 & 0 & 0 \end{bmatrix} \tag{16b}$$

where $\Phi(\bullet)$ is the Heaviside's function ($\Phi=0$ for $\bullet<0$; $\Phi=1$ for $\bullet\geq 0$). Fig. 5 depicts the non-null terms of these matrixes.

The resonant part of the effect $E'_{Di}(r;t)$ is defined as:

$$E'_{Di}(r;t) = \sum_{j=1}^{n} E'_{Dij}(r;t) \;;$$

$$E'_{Dij}(r;t) = \sum_{\kappa=1}^{6} \int_0^{Hp} F'_{Dpj\kappa}(z;t)\,\eta_{pi\kappa}(z,r)\,dz + \sum_{\kappa=1}^{6} \int_{-R}^{L} F'_{Ddj\kappa}(y;t)\,\eta_{di\kappa}(y,r)\,dy \tag{17}$$

where $E'_{Dij}(r;t)$ is the resonant part of the effect due to the $j$-th mode of vibration ($j=1,..n$); $F'_{Dpj\kappa}$ and $F'_{Ddj\kappa}$ are the $\kappa$-th components of the inertial actions that, applied quasi-statically and simultaneously along the pier and along the deck, respectively, induce the $j$-th resonant response of the $i$-th internal force. They are given by:

$$F'_{Dpj\kappa}(z;t) = \mu_{p\kappa}(z)(2\pi n_j)^2 \psi_{pj\kappa}(z) p_{Dj}(t) \tag{18a}$$

$$F'_{Ddj\kappa}(y;t) = \mu_{d\kappa}(y)(2\pi n_j)^2 \psi_{dj\kappa}(y) p_{Dj}(t) \tag{18b}$$

where $n_j$ is the $j$-th natural frequency; $\psi_{pj\kappa}(z)$ and $\psi_{dj\kappa}(y)$ are the $\kappa$-component of the $j$-th mode of vibration pertinent to the pier and to the deck, respectively; $p_{Dj}$ is the resonant part of the $j$-th

| Equation | Function |
|---|---|
| $\eta_{p11} = \Phi(z\text{-}r)$ | 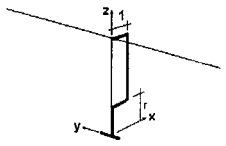 |
| $\eta_{p22} = \Phi(z\text{-}r)$ | 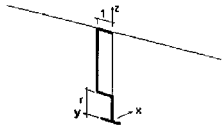 |
| $\eta_{p33} = \Phi(z\text{-}r)$ | 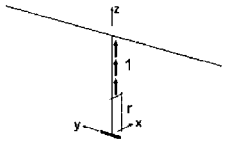 |
| $\eta_{p42} = -(z\text{-}r)\Phi(z\text{-}r)$ | 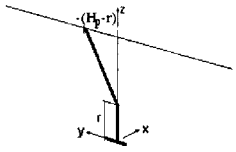 |
| | |
| $\eta_{p51} = (z\text{-}r)\Phi(z\text{-}r)$ | 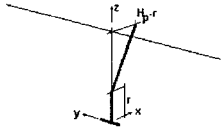 |
| | |
| $\eta_{p66} = \Phi(z\text{-}r)$ | 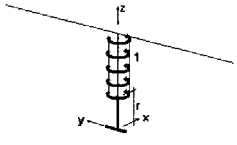 |

(a)

| Equation | Function |
|---|---|
| $\eta_{d11} = 1$ | 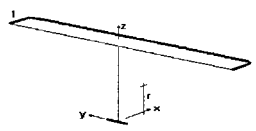 |
| $\eta_{d22} = 1$ | 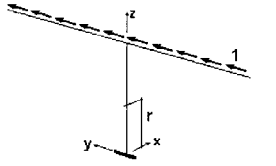 |
| $\eta_{d33} = 1$ | 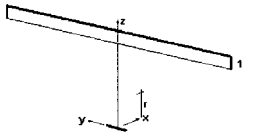 |
| $\eta_{d42} = -(H_d\text{-}r)$ | 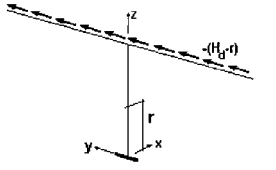 |
| $\eta_{d43} = y$ | 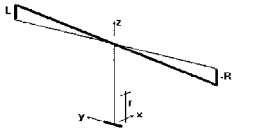 |
| $\eta_{d51} = H_d\text{-}r$ | 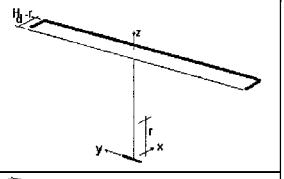 |
| $\eta_{d55} = 1$ | 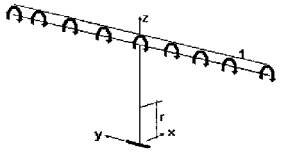 |
| $\eta_{d61} = -y$ | 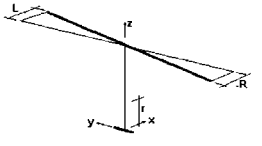 |

(b)

Fig. 5 Influence functions for the pier (a) and for the deck (b)

modal coordinate; $\mu_{p\kappa}$ and $\mu_{d\kappa}$ are, respectively, the $\kappa$-th component masses of the pier and of the deck per unit length; they denote translational ($\kappa=1,2,3$) or rotational ($\kappa=4,5,6$) masses according to whether $\psi_{pj\kappa}(z)$ and $\psi_{dj\kappa}(y)$ are translational or rotational parts of the mode. Replacing Eq. (18) into Eq. (17) provides:

$$E'_{Dij}(r,t) = (2\pi n_j)^2 p_{Dj}(t) m_{ij}(r) \tag{19}$$

where $m_{ij}$ is the influence effect mass of the structure for the $j$-th mode of vibration:

$$m_{ij}(r) = \sum_{\kappa=1}^{6} m_{ij\kappa}(r) \;;$$

$$m_{ij\kappa}(r) = \int_0^{H_p} \mu_{p\kappa}(z)\psi_{pj\kappa}(z)\eta_{pi\kappa}(z,r)dz + \int_{-R}^{L} \mu_{d\kappa}(y)\psi_{dj\kappa}(y)\eta_{di\kappa}(y,r)dy \tag{20}$$

Fig. 6 shows the shape of the four modes of vibration that usually cause the most relevant resonant effects on the bridge pier during construction. Their expressions may be given by the matrixes:

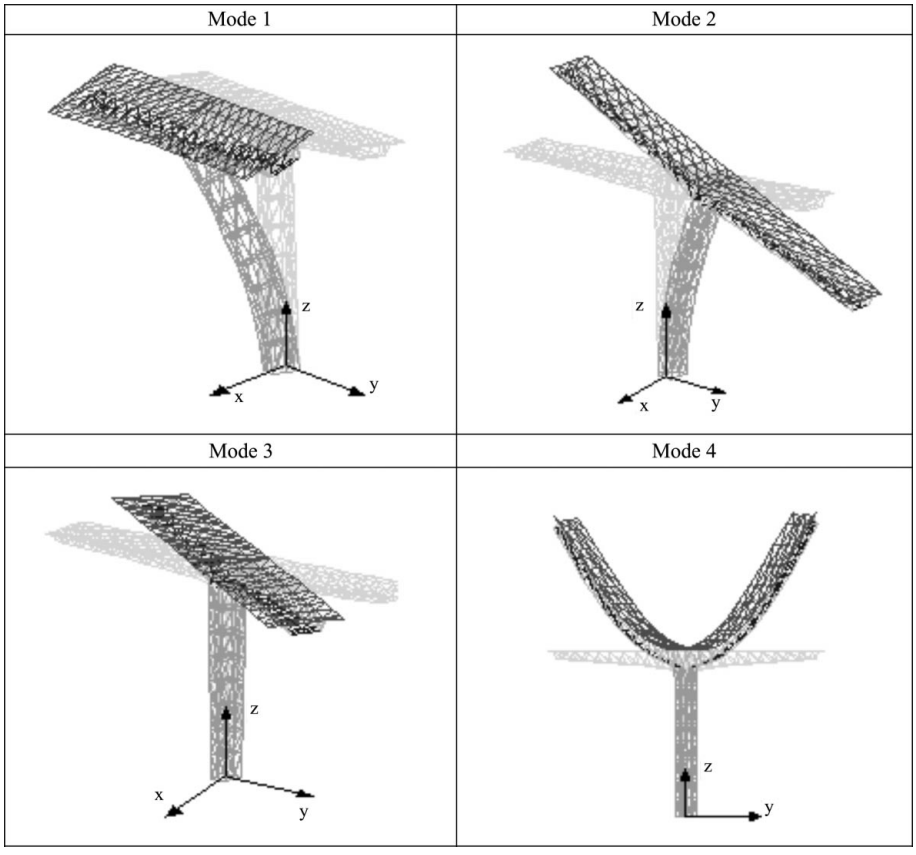


Fig. 6 Most relevant modes of vibration

$$[\psi_p(z)] = \begin{bmatrix} (z/H_p)^{\zeta_1} & 0 & 0 & 0 & 0 & 0 \\ 0 & (z/H_p)^{\zeta_2} & 0 & 0 & 0 & 0 \\ 0 & 0 & 0 & 0 & 0 & (z/H_p)^{\zeta_3} \\ 0 & 0 & 0 & 0 & 0 & 0 \end{bmatrix} \tag{21a}$$

$$[\psi_d(y)] = \begin{bmatrix} (H_d/H_p)^{\zeta_1} & 0 & 0 & 0 & \zeta_1(H_d/H_p)^{\zeta_1}/H_d & 0 \\ 0 & (H_d/H_p)^{\zeta_2} & -y\zeta_2(H_d/H_p)^{\zeta_2}/H_d & 0 & 0 & 0 \\ y(H_d/H_p)^{\zeta_3} & 0 & 0 & 0 & 0 & 0 \\ 0 & 0 & (|y|/R)^{\zeta_4} & 0 & 0 & 0 \end{bmatrix} \tag{21b}$$

whose $\kappa$, $j$-th terms are, respectively, $\psi_{pj\kappa}(z)$ and $\psi_{dj\kappa}(y)$ ; $\zeta_1$, $\zeta_2$, $\zeta_3$ and $\zeta_4$ are suitable nondimensional coefficients providing the shape of the modes.

## 4. Maximum effects

Assuming that damping is small and natural frequencies of similar modes are well separated, the mean value of the maximum effect $E_i$ during the period $T$ over which the wind velocity is averaged may be expressed as :

$$\bar{E}_{i,\max}(r) = \left|\bar{E}_i(r)\right| + g_i(r) \cdot \sqrt{\sigma_{Qi}^2(r) + \sum_{j=1}^{n} \sigma_{Dij}^2(r)} \tag{22}$$

where $\sigma_{Qi}(r)$ and $\sigma_{Dij}(r)$ are the rms values of $E'_{Qi}(r;t)$ and $E'_{Dij}(r;t)$, respectively; $g_i(r)$ is the peak factor, defined as :

$$g_i(r) = \sqrt{2\ln[\nu_i(r)T]} + \frac{0.5772}{\sqrt{2\ln[\nu_i(r)T]}} \tag{23}$$

where $\nu_i$ is the zero-up-crossing frequency given by the relationship :

$$\nu_i(r) = \sqrt{\frac{\sum_{j=1}^{n} n_j^2 \sigma_{Dij}^2(r)}{\sigma_{Qi}^2(r) + \sum_{j=1}^{n} \sigma_{Dij}^2(r)}} \tag{24}$$

which results sufficiently accurate for flexible structures, as those studied here, i.e. structures where the background part of the velocity is much lower than the resonant part.

The variance of the quasi-static part of the effect is given by:

$$\sigma_{Qi}^2(r) = \int_0^\infty S_{Ei}(r;n)dn \tag{25}$$

where $S_{Ei}(r;n)$ is the psdf of $E'_{Qi}(r;t)$:

$$\begin{aligned} S_{Ei}(r;n) = \sum_{\kappa=1}^{6}\sum_{\delta=1}^{6}\Bigg[ & \int_0^{H_p}\int_0^{H_p} S_{Fp\kappa Fp\delta}(z,z';n)\eta_{pi\kappa}(z,r)\eta_{pi\delta}(z',r)dzdz' \\ & + \int_{-R}^{L}\int_{-R}^{L} S_{Fd\kappa Fd\delta}(y,y';n)\eta_{di\kappa}(y,r)\eta_{di\delta}(y',r)dydy' \\ & + 2\int_0^{H_p}\int_{-R}^{L} S_{Fp\kappa Fd\delta}(z,y;n)\eta_{pi\kappa}(z)\eta_{di\delta}(y)dzdy\Bigg] \end{aligned} \tag{26}$$

where $\delta = 1,2,3$ correspond to forces along $x,y,z$ and $\delta = 4,5,6$ correspond to moments around $x,y,z$; $S_{Fp\kappa Fp\delta}(z,z';n)$ is the cpsdf of $F'_{p\kappa}(z;t)$ and $F'_{p\delta}(z';t)$, $S_{Fd\kappa Fd\delta}(y,y';n)$ is the cpsdf of $F'_{d\kappa}(y;t)$ and $F'_{d\delta}(y';t)$, $S_{Fp\kappa Fd\delta}(z,y;n)$ is the cpsdf of $F'_{p\kappa}(z;t)$ and $F'_{d\delta}(y;t)$ (Eq. (4)). These quantities are defined as:

$$S_{Fp\kappa Fp\delta}(z,z';n) = \sum\nolimits_{\varepsilon} \overline{f}_{p\kappa\varepsilon}(z)\overline{f}_{p\delta\varepsilon}(z')S_{\varepsilon}^{*}(M_p, M'_p; n) \tag{27a}$$

$$S_{Fd\kappa Fd\delta}(y,y';n) = \sum\nolimits_{\varepsilon} \overline{f}_{d\kappa\varepsilon}(y)\overline{f}_{d\delta\varepsilon}(y')S_{\varepsilon}^{*}(M_d, M'_d; n) \tag{27b}$$

$$S_{Fp\kappa Fd\delta}(z,y;n) = \sum\nolimits_{\varepsilon} \overline{f}_{p\kappa\varepsilon}(z)\overline{f}_{d\delta\varepsilon}(y)S_{\varepsilon}^{*}(M_p, M_d; n) \tag{27c}$$

where $\varepsilon = u,v,w,s$; $M_p \equiv (0;z)$, $M'_p \equiv (0;z')$, $M_d \equiv (y;H_d)$ and $M'_d \equiv (y';H_d)$; $\overline{f}_{p\alpha\varepsilon}(z)$ and $\overline{f}_{d\alpha\varepsilon}(y)$ are defined as:

$$\overline{f}_{p\kappa\varepsilon}(z) = \frac{1}{2}\rho\bar{u}^2(z)b_p\lambda_{p\kappa}c_{p\kappa\varepsilon}\gamma_{p\kappa\varepsilon}(z)J_{\varepsilon}(z) \tag{28a}$$

$$\overline{f}_{d\kappa\varepsilon}(y) = \frac{1}{2}\rho\bar{u}^2(H_d)b_d\lambda_{d\kappa}c_{d\kappa\varepsilon}\gamma_{d\kappa\varepsilon}(y)J_{\varepsilon}(H_d) \tag{28b}$$

Special expedients should be used to solve Eq. (25), especially with reference to the upper limit of integration with regard to the contribution of the vortex wake Piccardo and Solari (2000).

The variance of the $j$-th resonant part of the effect is given by:

$$\sigma_{Dij}^2(r) = \left[\frac{m_{ij}(r)}{\overline{m}_j}\right]^2 \frac{\pi n_j}{4\xi_j}\cdot S_{pDj}(n_j) \tag{29}$$

where $\xi_j$ is the damping coefficient of the $j$-th mode of vibration; $\overline{m}_j$ is the $j$-th modal mass:

$$\overline{m}_j = \sum_{\kappa=1}^{6}\overline{m}_{j\kappa} \;;\; \overline{m}_{j\kappa} = \int_0^{H_p}\mu_{p\kappa}(z)\psi_{pj\kappa}^2(z)dz + \int_{-R}^{L}\mu_{d\kappa}(y)\psi_{dj\kappa}^2(z)dy \tag{30}$$

$S_{pDj}(n_j)$ is the psdf of $p_{Dj}(r)$ :

$$S_{pDj}(n) = \sum_{\kappa=1}^{6}\sum_{\delta=1}^{6}\left[\int_0^{H_p}\int_0^{H_p} S_{Fp\kappa Fp\delta}(z,z';n)\,\psi_{pj\kappa}(z)\,\psi_{pj\delta}(z')\,dzdz'\right.$$

$$\left.+\int_{-R}^{L}\int_{-R}^{L} S_{Fd\kappa Fd\delta}(y,y';n)\,\psi_{dj\kappa}(y)\,\psi_{dj\delta}(y')\,dydy' + 2\int_0^{H_p}\int_{-R}^{L} S_{Fp\kappa Fd\delta}(z,y;n)\,\psi_{pj\kappa}(z)\,\psi_{dj\delta}(y)\,dzdy\right] \quad (31)$$

Aeroelastic effects may be included into this framework by expressing the modal damping coefficients as the sum of a structural part and of an aerodynamic part. Lock-in phenomena caused by the resonant shedding of vortices along the pier seem to be almost impossible due to the large mass at the top constituted by the cantilever deck arms. Lock-in phenomena caused by the resonant shedding of vortices along the arms seem to be not so frequent due to the high Scruton number of reinforced concrete decks, $Sc_d = 4\pi\overline{m}_d\xi_d/(\rho\bar{b}_d^2)$, where $\overline{m}_d$ and $\bar{b}_d$ are, respectively, the average mass per unit length and the average width of the tip third). However, they may be considered through the non linear aerodynamic damping model proposed by Vickery & Basu (1983).

An example of the calculation of the effect $E_1$ is provided in Appendix I. All other effects may be determined analogously (Schmidt 2001).

The gust factor $G_i(r)$ is defined traditionally as the ratio between the mean value of the maximum effect $\bar{E}_{i,\max}(r)$ and the mean effect $\bar{E}_i(r)$. However, this method cannot be applied in this case, since some mean effects could be zero. To circumvent this difficulty and to retain the use of a quantity which is quite representative from an engineering viewpoint, the following gust effect factors will be calculated :

$$G_i(r) = \bar{E}_{i,\max}(r)/E^*(r) \quad (32)$$

where $E^*(r) = \bar{E}_1(r)$ for $i=1,2,3$ and $E^*(r) = \bar{E}_5(r)$ for $i=4,5,6$.

## 5. Applications

The application and the implications of the proposed model are illustrated with reference to the Otira Viaduct and the Limassol - Paphos bridge. The Otira Viaduct is a cast-in-place bridge built in balanced-cantilever stages using form travellers. It consists of four spans measuring 87, 134, 134, and 87 m for a total length of 442 m; it carries Highway 73 through the Arthur's National Park in New Zealand. The Limassol - Paphos bridge in the Republic of Cyprus was erected in balanced-cantilever stages using a self-launching overhead gantry to place the precast segments. It consists of five spans measuring 38.5, 55, 55, 55 and 38.5 m. Fig. 7 shows the geometry of the two bridges during the worst balance-erection stage. Table 1 provides a list of main structural parameters. Table 2 shows, for each bridge, the modal properties associated with the modal shapes depicted in Fig. 6. Table 3 lists the main aerodynamic parameters as derived from literature; much better results may be obtained through wind tunnel tests.

Both structures are built on an homogenous terrain with a roughness length $z_0 = 0.05$ m. The mean

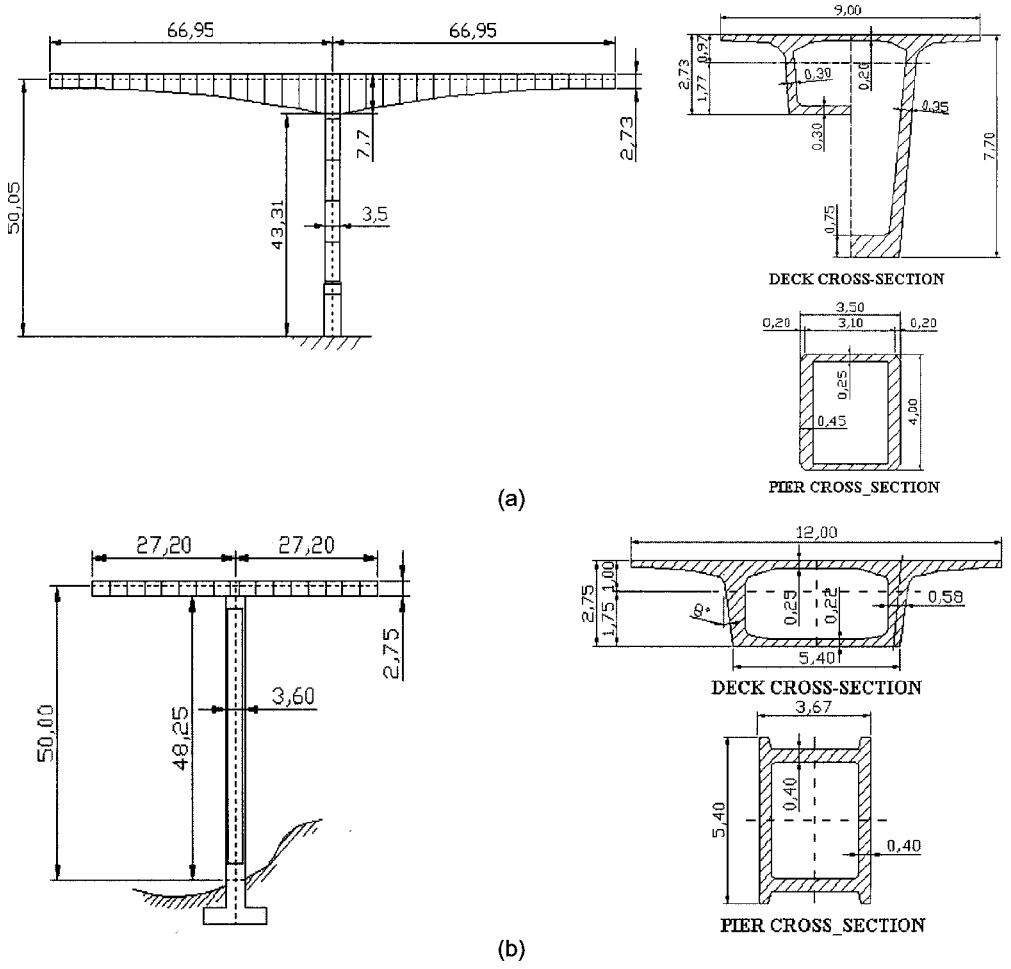


Fig. 7 Geometry of the Otira Viaduct, New Zealand (a) and of the Limassol-Paphos Bridge, Republic of Cyprus (b)

Table 1 Main structural parameters

| | Parameters | Otira Viaduct | Limassol - Paphos Bridge |
|---|---|---|---|
| Pier | Height [m] | $H_p$ = 43.3 | $H_p$ = 48.25 |
| | Width [m] | $b_p$ = 3.50 | $b_p$ = 3.60 |
| | Mass [kg/m] | $m_p$ = 12000 | $m_p$ = 16250 |
| Deck | Cantil. lengths [m] | $L = R$ = 66.95 | $L = R$ = 27.20 |
| | Height [m] | $H_d$ = 50.0 | $H_d$ = 50.0 |
| | Width [m] | $b_d(y) = 7.70-5.00(\|y\|/R)^{0.5}$ | $b_d(y)$ = 2.75 |
| | Mass [kg/m] | $m_d(y) = 24400-12200(\|y\|/R)^{0.5}$ | $m_d(y)$ = 19300 |

wind velocity profile is described by the power law $\bar{u}(z)=u_{ref}(z/H_p)^{\beta}$, where $\beta=0.16$, $u_{ref}=\bar{u}(H_p)$ and $T=10$ minutes. The integral length scales of the three turbulence components are $L_u(z)=$

Table 2 Modal properties

| $j$ | Otira Viaduct | | | Limassol - Paphos Bridge | | |
|---|---|---|---|---|---|---|
| | Nat. frequ. $n_j$ [Hz] | Structural damping $\xi_j$ | Shape factor $\zeta_j$ | Nat. frequ. $n_j$ [Hz] | Structural damping $\xi_j$ | Shape factor $\zeta_j$ |
| 1 | 0.33 | 0.01 | 1.7 | 0.48 | 0.01 | 1.7 |
| 2 | 0.15 | 0.01 | 1.9 | 0.35 | 0.01 | 1.8 |
| 3 | 0.14 | 0.01 | 1.0 | 0.45 | 0.01 | 1.0 |
| 4 | 1.54 | 0.01 | 2.0 | 3.50 | 0.01 | 1.4 |

Table 3 Main aerodynamic parameters

| | Parameters | Otira Viaduct | Limassol - Paphos Bridge |
|---|---|---|---|
| Pier | $c_{dp}$ | 1.50 | 1.70 |
| | $c'_{lp}$ | -4.10 | -4.00 |
| | $c'_{mp}$ | 0.40 | 0.50 |
| | $\tilde{c}_{lsp}$ | 0.50 | 0.50 |
| | $\tilde{c}_{msp}$ | 0.04 | 0.03 |
| | $S_p$ | 0.11 | 0.10 |
| Deck | $c_{dd}$ | 1.60 | 1.80 |
| | $c'_{dd}$ | -0.20 | 0.00 |
| | $\tilde{c}_{lsd}$ | 0.06 | 0.10 |
| | $c_{ld}$ | 2.30 | 1.50 |
| | $c'_{ld}$ | 9.00 | 15.00 |
| | $\tilde{c}_{msd}$ | 0.07 | 0.10 |
| | $c_{md}$ | 2.75 | 1.00 |
| | $c'_{md}$ | -1.85 | 2.00 |
| | $S_d$ | 0.15 | 0.15 |

$300\,(z/300)^{\varepsilon}$, $L_v(z)=0.25L_u(z)$ and $L_w(z)=0.10L_u(z)$, where $\varepsilon=0.26$; the turbulence intensities are $I_u(z)=1/\ln(z/z_0)$, $I_v(z)=0.75I_u(z)$ and $I_w(z)=0.50I_u(z)$; the exponential decay coefficients are: $C_{yu}=C_{zu}=10$, $C_{yv}=C_{yw}=C_{zv}=6.5$, $C_{zw}=3$ (Solari and Piccardo 2001). $\mathcal{L}_q=1$; $Y_{q\theta}=0.9$, $B^2_{q\kappa}(z) = B^2_{0\kappa} + 2I^2_u(z)$ $(q= p,d)$, $B_{0\kappa}=0.08$.

Wind-induced internal forces along the pier were evaluated by implementing the method described above within the computer program MathCAD 2000 Professional.

Table 4(a) shows the main results of the analysis of the wind-induced response of the Otira Viaduct for $u_{ref}=26.0$ m/s. Tables 4(b) and 4(c) show the main results of the analysis of the wind-induced response of the Limassol-Paphos Bridge for $u_{ref}=12.0$ m/s and $u_{ref}=26.0$ m/s, respectively. All tables point out, for each internal force at the base of the pier, the different contributions related to the mean static part, to the quasi-static part and to the resonant part for each mode considered. It is apparent that each mode in Fig. 6 contributes to the resonant part of only one effect.

Lock-in effects due to the resonant shedding of vortices along the cantilever deck arms may be ignored due to the high Scruton numbers, $Sc_d=135$ and $Sc_d=256$, involved by the Otira Viaduct

Table 4 (a) Wind-induced internal forces at the base of the pier of the Otira Viaduct for $u_{ref}$ = 26.0 m/s

| $i$ | $\lvert\overline{E}_i\rvert$ | $\sigma_{Qi}$ | $\sigma_{D1}$ | $\sigma_{D2}$ | $\sigma_{D3}$ | $\sigma_{D4}$ | $\nu_i$ [Hz] | $g_i$ | $\overline{E}_{i,\max}$ | $G_i$ |
|---|---|---|---|---|---|---|---|---|---|---|
| 1 | 4.89E+05 N | 1.16E+05 | 1.68E+05 | 0 | 0 | 0 | 0.27 | 3.37 | 1.18E+06 N | 2.41 |
| 2 | 0 | 1.18E+04 | 0 | 1.88E+05 | 0 | 0 | 0.15 | 3.19 | 6.01E+05 N | 1.23 |
| 3 | 5.98E+05 N | 1.83E+05 | 0 | 0 | 0 | 6.91E+04 | 0.55 | 3.57 | 1.30E+06 N | 2.65 |
| 4 | 0 | 2.29E+06 | 0 | 1.78E+07 | 0 | 0 | 0.15 | 3.19 | 5.73E+07 Nm | 2.21 |
| 5 | 2.59E+07 Nm | 6.11E+06 | 8.21E+06 | 0 | 0 | 0 | 0.27 | 3.37 | 6.04E+07 Nm | 2.33 |
| 6 | 0 | 1.20E+06 | 0 | 0 | 5.30E+06 | 0 | 0.16 | 3.21 | 1.74E+07 Nm | 0.67 |

(b) Wind-induced internal forces at the base of the pier of the Limassol - Paphos Bridge for $u_{ref}$ = 12.0 m/s

| $i$ | $\lvert\overline{E}_i\rvert$ | $\sigma_{Qi}$ | $\sigma_{D1}$ | $\sigma_{D2}$ | $\sigma_{D3}$ | $\sigma_{D4}$ | $\nu_i$ [Hz] | $g_i$ | $\overline{E}_{i,\max}$ | $G_i$ |
|---|---|---|---|---|---|---|---|---|---|---|
| 1 | 4.47E+04 N | 1.14E+04 | 5.33E+03 | 0 | 0 | 0 | 0.20 | 3.29 | 8.61E+04 N | 1.93 |
| 2 | 0 | 3.43E+03 | 0 | 1.64E+04 | 0 | 0 | 0.34 | 3.44 | 5.78E+04 N | 1.29 |
| 3 | 2.04E+04 N | 1.27E+04 | 0 | 0 | 0 | 3.13E+03 | 0.84 | 3.69 | 6.88E+04 N | 1.54 |
| 4 | 0 | 1.31E+05 | 0 | 8.91E+05 | 0 | 0 | 0.35 | 3.44 | 3.10E+06 Nm | 1.60 |
| 5 | 1.94E+06 Nm | 4.83E+05 | 2.51E+05 | 0 | 0 | 0 | 0.22 | 3.31 | 3.74E+06 Nm | 1.93 |
| 6 | 0 | 3.35E+04 | 0 | 0 | 6.07E+04 | 0 | 0.39 | 3.48 | 2.41E+05 Nm | 0.12 |

(c) Wind-induced internal forces at the base of the pier of the Limassol - Paphos Bridge for $u_{ref}$ = 26.0 m/s

| $i$ | $\lvert\overline{E}_i\rvert$ | $\sigma_{Qi}$ | $\sigma_{D1}$ | $\sigma_{D2}$ | $\sigma_{D3}$ | $\sigma_{D4}$ | $\nu_i$ [Hz] | $g_i$ | $\overline{E}_{i,\max}$ | $G_i$ |
|---|---|---|---|---|---|---|---|---|---|---|
| 1 | 2.10E+05 N | 5.37E+04 | 4.75E+04 | 0 | 0 | 0 | 0.32 | 3.42 | 4.55E+05 N | 2.17 |
| 2 | 0 | 1.24E+04 | 0 | 6.68E+04 | 0 | 0 | 0.34 | 3.44 | 2.34E+05 N | 1.12 |
| 3 | 9.59E+04 N | 5.97E+04 | 0 | 0 | 0 | 2.71E+04 | 1.45 | 3.84 | 3.48E+05 N | 1.66 |
| 4 | 0 | 4.91E+05 | 0 | 3.62E+06 | 0 | 0 | 0.35 | 3.44 | 1.26E+07 Nm | 1.38 |
| 5 | 9.10E+06 Nm | 2.26E+06 | 2.23E+06 | 0 | 0 | 0 | 0.34 | 3.44 | 2.00E+07 Nm | 2.20 |
| 6 | 0 | 1.50E+05 | 0 | 0 | 4.73E+05 | 0 | 0.43 | 3.51 | 1.74E+06 Nm | 0.19 |

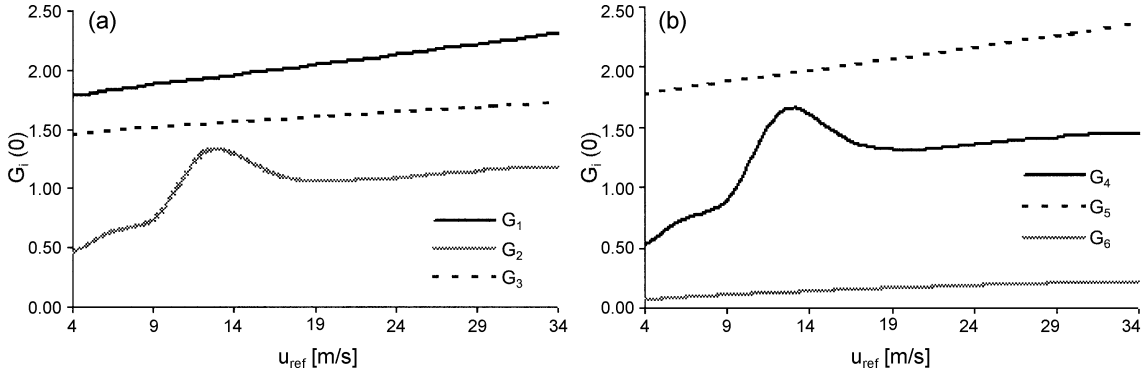


Fig. 8 Gust effect factors at the base of the pier of the Limassol-Paphos Bridge

and by the Limassol-Paphos Bridge, respectively.

Fig. 8 refers to the Limassol-Paphos Bridge and depicts the dependence of the gust effect factors

Table 5 (a) Percent contributions of different loading components corresponding to Table 4(a)

| | $\overline{E}_{1,\max}$ | $\overline{E}_{2,\max}$ | $\overline{E}_{3,\max}$ | $\overline{E}_{4,\max}$ | $\overline{E}_{5,\max}$ | $\overline{E}_{6,\max}$ |
|---|---|---|---|---|---|---|
| $\overline{u}_p$ | 6 | 0 | 0 | 0 | 3 | 0 |
| $\overline{u}_d$ | 35 | 0 | 46 | 0 | 40 | 0 |
| $u'_p$ | 7 | 0 | 0 | 0 | 4 | 0 |
| $u'_d$ | 39 | 25 | 27 | 26 | 41 | 75 |
| $v'_p$ | 0 | 1 | 0 | 0 | 0 | 0 |
| $w'_d$ | 13 | 74 | 26 | 74 | 12 | 25 |
| $s'_p$ | 0 | 0 | 0 | 0 | 0 | 0 |
| $s'_d$ | 0 | 0 | 1 | 0 | 0 | 0 |

(b) Percent contributions of different loading components corresponding to Table 4(b)

| | $\overline{E}_{1,\max}$ | $\overline{E}_{2,\max}$ | $\overline{E}_{3,\max}$ | $\overline{E}_{4,\max}$ | $\overline{E}_{5,\max}$ | $\overline{E}_{6,\max}$ |
|---|---|---|---|---|---|---|
| $\overline{u}_p$ | 23 | 0 | 0 | 0 | 15 | 0 |
| $\overline{u}_d$ | 29 | 0 | 30 | 0 | 37 | 0 |
| $u'_p$ | 30 | 0 | 0 | 0 | 21 | 0 |
| $u'_d$ | 17 | 1 | 10 | 1 | 26 | 86 |
| $v'_p$ | 0 | 3 | 0 | 1 | 0 | 0 |
| $w'_d$ | 1 | 35 | 60 | 37 | 1 | 14 |
| $s'_p$ | 0 | 61 | 0 | 61 | 0 | 0 |
| $s'_d$ | 0 | 0 | 0 | 0 | 0 | 0 |

(c) Percent contributions of different loading components corresponding to Table 4(c)

| | $\overline{E}_{1,\max}$ | $\overline{E}_{2,\max}$ | $\overline{E}_{3,\max}$ | $\overline{E}_{4,\max}$ | $\overline{E}_{5,\max}$ | $\overline{E}_{6,\max}$ |
|---|---|---|---|---|---|---|
| $\overline{u}_p$ | 21 | 0 | 0 | 0 | 13 | 0 |
| $\overline{u}_d$ | 25 | 0 | 27 | 0 | 33 | 0 |
| $u'_p$ | 27 | 0 | 0 | 0 | 19 | 0 |
| $u'_d$ | 25 | 4 | 10 | 4 | 33 | 87 |
| $v'_p$ | 0 | 6 | 0 | 4 | 0 | 0 |
| $w'_d$ | 2 | 90 | 63 | 92 | 2 | 13 |
| $s'_p$ | 0 | 0 | 0 | 0 | 0 | 0 |
| $s'_d$ | 0 | 0 | 0 | 0 | 0 | 0 |

Table 6 Bending moments $E_4$ at the pier bases in accordance with AASHTO

| | $E^*_{4d}$ [kNm] | $E^*_{4p}$ [kNm] | $E^*_4$ [kNm] | $\overline{E}_{4,\max}$ [kNm] | $\frac{\overline{E}_{4,\max}}{E^*_4}$ |
|---|---|---|---|---|---|
| Otira Viaduct ($u_{ref}$ = 26.0 m/s) | 4836 | 5474 | 10310 | 57300 | 5.56 |
| Paphos Bridge ($u_{ref}$ = 12.0 m/s) | 1061 | 1960 | 3021 | 3100 | 1.03 |
| Paphos Bridge ($u_{ref}$ = 26.0 m/s) | 1061 | 9179 | 10240 | 12600 | 1.23 |

$G_i(0)$ (Eq. (32)) on the mean wind velocity $u_{ref}$. It stresses that $u_{ref} = 12$ m/s induces a vortex shedding along the pier, resonant with the second mode of vibration (Table 4(b)).

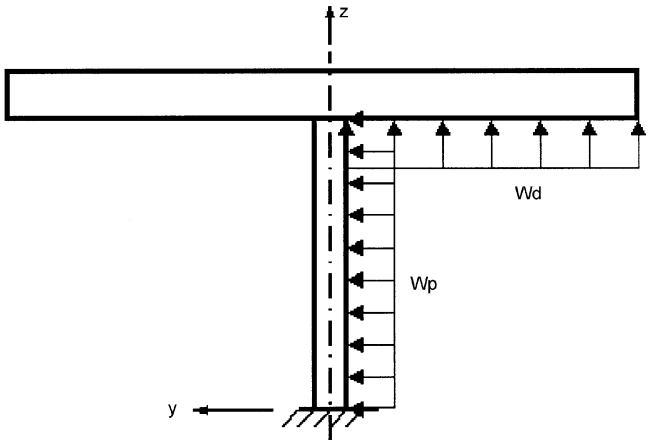


Fig. 9 AASHTO conventional load to take into account out-of-balance conditions

Tables 5(a), 5(b) and 5(c) correspond to Tables 4(a), 4(b) and 4(c), respectively. They show, for each internal force, the contributions provided by the static actions due to the mean wind velocity ($\bar{u}$) and by the fluctuating actions due to the three turbulence components ($u'$, $v'$, $w'$) and to the wake excitation ($s'$). The contributions due to $\bar{u}$, $u'$ and $s'$ are splitted between the pier and the deck to show the influence of each element. The turbulence components $v'$ and $w'$ cause actions only on the pier and on the deck, respectively. The sum of the contributions in each column provides the 100% of $\bar{E}_{i,\max}$. Grey boxes denote effects and loading components taken into account by previous analyses concerning this topic (Dyrbye and Hansen 1997; Mendes and Branco 2001). It is apparent that neglecting other effects and other loading components oversimplifies the problem and underestimates the final results.

The same concept applies to AASHTO Specifications (AASHTO 1996). They recommend a conventional load to take into account out-of-balance conditions that may produce a crucial bending moment around $x$-axis ($E_4^*$) at the base of the pier. Adopting the scheme in Fig. 9, $w_d = 0.24$ kN/m$^2$ (5 psf) is an uplift load on one cantilever arm; $w_p = w_{pb}K^2$, where $w_{pb} = 1.92$ kN/m$^2$ (40 psf) is a uniform pressure over the pier, corresponding to a base wind velocity $u_b = 44.7$ m/s (100 mph), $K = u_p/u_b$ where $u_p \sim 1.5u_{ref}$ is the peak value of the design wind velocity; $E_4^* = E_{4d}^* + E_{4p}^*$, where $E_{4d}^*$ and $E_{4p}^*$ are the base bending moments, around $x$-axis, due to $w_d$ and to $w_p$, respectively. Table 5 shows a comparison between the results provided by the proposed method and by AASHTO Specifications. It is apparent that these specifications are easy to apply but their results are very rough and, in some cases, extremely unsafe. Since balanced cantilever erection is quite common in the United States, particular concern emerges from the application of AASHTO method to calculate the wind-induced effects of bridges involving this erection technique.

## 6. Conclusions

A general method has been formulated to determine the wind-induced effects during balanced cantilever erection stages of bridges. The structure is immersed in a wind field characterised by a mean wind velocity profile orthogonal to the bridge plane and by a 3-D turbulent model.

Aerodynamic actions on the pier and on the deck arms are schematised as the sum of the actions due to the oncoming wind flow, i.e., to the mean wind velocity and to the longitudinal, lateral and vertical turbulence components, and to the vortex wakes. The structure has a linear elastic behaviour with viscous damping. Geometrical, mechanical and aerodynamic properties of the bridge are modeled in such a way as to guarantee a broad band of applications in the engineering sector. The model provides the statistical parameters of the six components of the internal forces along the pier, i.e., the normal force, two orthogonal shear forces and bending moments, and the torque. Each effect takes into account the static part, the quasi-static part and the resonant part of the response. The static and the quasi-static parts are calculated by the influence function technique, i.e., by taking all vibration modes into account. The resonant part of the response is determined by selecting the most significant modes of vibration. Effects along the deck may be easily determined by generalising the methods described in (Piccardo and Solari 2002) from cantilever vertical structures to cantilever horizontal structures.

This model represents an extreme generalisation of the previous methods suggested by code provisions (AASHTO 1996), textbooks (Dyrbye and Hansen 1997) and scientific papers (Mendes and Branco 2001). They enabled to take into consideration only a limited sub-set of the complex phenomena induced by wind on bridges during balanced cantilever erection stages. The comparison between previous partial approaches and the more general method developed here demonstrates that several effects traditionally disregarded may play a fundamental role depending on the properties of the structure considered and that current techniques may involve unsafe evaluations.

These considerations agree with the experimental research carried out in (Aas-Jakobsen, Strϕmmen 1999), where wind-induced accelerations at the tip of the arms of a bridge during balanced cantilever erection were measured. The primary conclusion was that the vortex shedding caused by moderate mean wind velocities may produce significant vertical movements of cantilever arms.

The model formulated and the results obtained suggest a lot of perspectives for improving and extending this work. First, it is apparent that, after assessing a theoretical model, wind tunnel tests and full-scale measurements should be carried out to check and calibrate the procedure or, at least, to estimate the aerodynamic model parameters. Second, it should be pointed out that the present approach is so complex as to require its implementation in a computer; in the perspective of making its use more user-friendly in the engineering sector and for applications into standards and codes, closed form solutions like those developed for cantilever vertical structures (Piccardo and Solari 1998; 2000; 2002) should be very appropriate. Third, this method provides information on the single components of the internal forces along the pier; further analyses aimed at evaluating combination rules based on cross-correlation statistical properties are fundamental to complete the model. Finally, generalising this model to the erection stages of cable-stayed bridges including aeroelastic effects should be very appealing. Concerns are currently addressed to all these developments.

## Acknowledgements

The authors are indebted to Parsons Bridge and Tunnel Division, Denver, USA and to Rizzani de Eccher S.p.A., Udine, Italy for having supported this research with project data. Special thanks are due to Prof. C. Bucher of Bauhaus-University Weimar, Germany, for his interest and encouragement

towards this work.

## References

AASHTO (1996), *Standard Specifications for Highway Bridges*, 16th Edition, American Association for State Highway and Transportation Officials.

Aas-Jakobsen K., Strϕmmen E. (1999), "Dynamic response of a box girder bridge during construction", *Proc., 10th Int. Conf. on Wind Engineering*, Copenhagen, 827-832.

Davenport, A.G. (1995), "How can we simplify and generalize wind loads", *J. Wind Eng. Ind. Aerod.*, **54-55**, 657-669.

Dyrbye, C. and Hansen, S.O. (1997), *Wind Loads on Structures*. New York, Wiley.

Engineering Sciences Data Unit (1990), Dynamic response to vortex shedding. Part I: calculation procedures and derivation. ESDU Item 85038, London, U.K..

Holmes, J.D. (1994), "Along-wind response of lattice towers: part I - derivation of expressions for gust response factors", *Eng. Struct*., **16**, 287-292.

Holmes, J.D. (2002), "Effective static load distributions in wind engineering", *J. Wind Eng. Ind. Aerod.*, **90**, 91-109.

Kasperski, M. (1992), "Extreme wind load distributions for linear and nonlinear design", *Eng. Struct.*, **14**, 27-34.

Mendes, P.A. and Branco, F.A. (2001), "Unbalanced wind buffeting effects on brides during double cantilever erection stages", *Wind & Struct.*, **4**(1), 45-62.

Piccardo, G. and Solari, G. (1998), "Closed form prediction of 3-D wind-excited response of slender structures", *J. Wind Eng. Ind. Aerod.*, **74-76**, 697-708.

Piccardo, G. and Solari, G. (2000), "3-D wind-excited response of slender structures: Closed form solution", *J. Struct. Engng.*, ASCE, **126**(8), 936-943.

Piccardo, G. and Solari, G. (2002), "3-D gust effect factor for slender vertical structures", *Prob. Eng. Mech.*, **17**, 143-155.

Schmidt, S. (2001), "Wind-induced effects during balanced cantilever erection stages of bridges", Diploma Thesis, Bauhaus-University Weimar, Germany.

Solari, G. (1985), "Mathematical model to predict 3-D wind loading on buildings", *J. Eng. Mech.*, ASCE, **111**, 254-276.

Solari, G. and Piccardo, G. (2001), "Probabilistic 3-D turbulence modelling for gust buffeting of structures", *Prob. Eng. Mech.*, **16**, 73-86.

Solari, G. (1989), "Wind response spectrum", *J. Eng. Mech.*, ASCE, **115**, 2057-2073.

Vickery, B.J. and Basu, R.I. (1983), "Across-wind vibrations of structures of circular cross-section. Part I: development of a mathematical model for two-dimensional conditions; Part II: development of a mathematical model for full-scale application", *J. Wind Eng. Ind. Aerod.*, **12**, 49-74; 75-97.

Vickery, B.J. and Clark, W. (1972), "Lift or across-wind response of tapered stacks", *J. Struct. Div.*, ASCE, **98**, 1-20.

## Appendix I - Computation of $E_1$

The effect $E_1(r)$ is the alongwind shear force at height $r$ of the pier. Replacing Eq. (3) into Eq. (14), its mean value results :

$$\bar{E}_1(r) = \frac{1}{2}\rho b_p c_{dp}\int_r^{H_p}\bar{u}^2(z)\gamma_{p1u}(z)dz + \frac{1}{2}\rho b_d c_{dd}\int_{-R}^{L}\bar{u}^2(H_d)\gamma_{d1u}(y)dy \tag{33}$$

where the nondimensional functions $\gamma_{p1u}$ and $\gamma_{d1u}$ are given by:

$$\gamma_{p1u}(z) = \frac{b_p(z)}{b_p}\frac{c_{dp}(z)}{c_{dp}} \quad ; \quad \gamma_{d1u}(y) = \frac{b_d(y)}{b_d}\frac{c_{dd}(y)}{c_{dd}} \tag{34}$$

Based on Eqs. (25)~(28), the variance of the quasi-static part of $E_1$ is defined as:

$$\sigma^2_{Q1}(r) = \sigma^2_{Q1pu}(r) + \sigma^2_{Q1du}(r) + \sigma^2_{Q1dw}(r) + 2C_{Q1pdu}(r) \tag{35}$$

where $\sigma^2_{Q1pu}(r)$, $\sigma^2_{Q1du}(r)$ and $\sigma^2_{Q1dw}(r)$ are, respectively, the contributions due to the actions of the longitudinal turbulence over the pier and over the deck, and of the vertical turbulence over the deck; $C_{Q1pdu}(r)$ is the covariance of the actions of the longitudinal turbulence over the pier and over the deck:

$$\sigma^2_{Q1pu}(r) = \left[c_{dp}\frac{1}{2}\rho b_p\right]^2 \int_0^{n_1}\int_r^{H_p}\int_r^{H_p} \gamma_{p1u}(z)\gamma_{p1u}(z')\bar{u}^2(z)\bar{u}^2(z')J_u(z)J_u(z')S_u^*(M_p, M_p'; n)dzdz'dn \tag{36a}$$

$$\sigma^2_{Q1du}(r) = \left[\frac{1}{2}\rho\bar{u}^2(H_d)b_d c_{dd}J_u(H_d)\right]^2 \int_0^{n_1}\int_{-R}^{L}\int_{-R}^{L} \gamma_{d1u}(y)\gamma_{d1u}(y')S_u^*(M_d, M_d'; n)dydy'dn \tag{36b}$$

$$\sigma^2_{Q1dw}(r) = \left[\frac{1}{2}\rho\bar{u}^2(H_d)b_d(c_{dd}' - c_{ld})J_w(H_d)\right]^2 \int_0^{n_1}\int_{-R}^{L}\int_{-R}^{L} \gamma_{d1w}(y)\gamma_{d1w}(y')S_w^*(M_d, M_d'; n)dydy'dn \tag{36c}$$

$$C_{Q1pdu}(r) = \left[\frac{1}{4}c_{dp}c_{dd}\rho^2\bar{u}^2(H_d)J_u(H_d)b_p b_d\right]\int_0^{n_1}\int_r^{H_p}\int_{-R}^{L} \bar{u}^2(z)\gamma_{p1u}(z)\gamma_{d1u}(y)J_u(z)S_u^*(M_p, M_d'; n)dzdydn \tag{36d}$$

Based on Eqs. (29) - (31), the variance of the resonant part of $E_1$ is defined as:

$$[\sigma_{D11}(r)]^2 = \left[\frac{m_{11}(r)}{\bar{m}_1}\right]^2 \frac{\pi n_1}{4\xi_1} \cdot [S_{Dp111u}(n_1) + S_{Dd111u}(n_1) + S_{Dd111w}(n_1) + S_{Dd155u}(n_1) + S_{Dd155w}(n_1)$$
$$+ S_{Dp155s}(n_1) + 2\cdot S_{Dd115u}(n_1) + 2\cdot S_{Dd115w}(n_1) + 2\cdot S_{Dpd111u}(n_1) + 2\cdot S_{Dpd115u}(n_1)] \tag{37a}$$

$$\sigma^2_{D12}(r) = \sigma^2_{D13}(r) = \sigma^2_{D14}(r) = 0 \tag{37b}$$

where, Eq. (37b) applies for equal cantilever length($R$=$L$); furthermore, from Eqs. (20) and (30) :

$$m_{11}(r) = \int_r^{H_p}\mu_{p1}(z)(z/H_p)^{\zeta_1}dz + \int_{-R}^{L}\mu_{d1}(y)(H_d/H_p)^{\zeta_1}dy \tag{38}$$

$$\bar{m}_1(r) = \int_0^{H_p}\mu_{p1}(z)(z/H_p)^{2\zeta_1}dz + \int_{-R}^{L}\mu_{d1}(y)(H_d/H_p)^{2\zeta_1}dy + \int_{-R}^{L}\mu_{d5}(y)\zeta_1^2(H_d/H_p)^{2\zeta_1}/H_d^2 dy \tag{39}$$

$S_{Dp111u}$, $S_{Dd111u}$, $S_{Dd111w}$, $S_{Dd155u}$, $S_{Dd155w}$ and $S_{Dd155s}$ are, respectively, the contributions due to the actions of

the longitudinal turbulence over the pier and over the deck, and of the vertical turbulence over the deck; $S_{Dd115u}$, $S_{Dd115w}$, $S_{Dpd111u}$ and $S_{Dpd115u}$ are related to the cross-correlation of the actions of the longitudinal turbulence over the pier and over the deck:

$$S_{Dp111u}(n_1) = \frac{1}{4}\rho^2 b_p^2 c_{dp}^2 \int_0^{H_p}\int_0^{H_p} \gamma_{p1u}(z)\gamma_{p1u}(z')\bar{u}^2(z)\bar{u}^2(z')J_u(z)J_u(z')\left(\frac{z}{H_p}\right)^{\zeta_1}\left(\frac{z'}{H_p}\right)^{\zeta_1} S_u^*(M_p, M_p'; n_1)\,dz dz' \tag{40a}$$

$$S_{Dd111u}(n_1) = \frac{1}{4}\rho^2 \bar{u}^4(H_d) b_d^2 c_{dd}^2 J_u^2(H_d) \int_{-R}^{L}\int_{-R}^{L} \gamma_{d1u}(y)\gamma_{d1u}(y')(H_d/H_p)^{2\zeta_1} S_u^*(M_d, M_d'; n_1)\,dy dy' \tag{40b}$$

$$S_{Dd111w}(n_1) = \frac{1}{4}\rho^2 \bar{u}^4(H_d) b_d^2 (c_{dd}' - c_{ld})^2 J_w^2(H_d) \int_{-R}^{L}\int_{-R}^{L} \gamma_{d1w}(y)\gamma_{d1w}(y')(H_d/H_p)^{2\zeta_1} S_w^*(M_d, M_d'; n_1)\,dy dy' \tag{40c}$$

$$S_{Dd155u}(n_1) = \frac{1}{4}\rho^2 \bar{u}^4(H_d) b_d^4 c_{md}^2 J_u^2(H_d) \int_{-R}^{L}\int_{-R}^{L} \gamma_{d5u}(y)\gamma_{d5u}(y')\frac{\zeta_1^2}{H_d^2}(H_d/H_p)^{2\zeta_1} S_u^*(M_d, M_d'; n_1)\,dy dy' \tag{40d}$$

$$S_{Dd155w}(n_1) = \frac{1}{4}\rho^2 \bar{u}^4(H_d) b_d^4 c_{md}'^2 J_w^2(H_d) \int_{-R}^{L}\int_{-R}^{L} \gamma_{d5w}(y)\gamma_{d5w}(y')\frac{\zeta_1^2}{H_d^2}(H_d/H_p)^{2\zeta_1} S_w^*(M_d, M_d'; n_1)\,dy dy' \tag{40e}$$

$$S_{Dd155s}(n_1) = \frac{1}{4}\rho^2 \bar{u}^4(H_d) b_d^4 \tilde{c}_{msd}^2 \int_{-R}^{L}\int_{-R}^{L} \gamma_{d5s}(y)\gamma_{d5s}(y')\frac{\zeta_1^2}{H_d^2}(H_d/H_p)^{2\zeta_1} S_s^*(M_d, M_d'; n_1)\,dy dy' \tag{40f}$$

$$S_{Dd115u}(n_1) = \frac{1}{4}\rho^2 \bar{u}^4(H_d) J_u^2(H_d) b_d^3 c_{dd} c_{md} \int_{-R}^{L}\int_{-R}^{L} \gamma_{d1u}(y)\gamma_{d5u}(y')\frac{\zeta_1}{H_d}(H_d/H_p)^{2\zeta_1} S_u^*(M_d, M_d'; n_1)\,dy dy' \tag{40g}$$

$$S_{Dd115w}(n_1) = \frac{1}{4}\rho^2 \bar{u}^4(H_d) J_w^2(H_d) b_d^3 (c_{dd}' - c_{ld}) c_{md}' \int_{-R}^{L}\int_{-R}^{L} \gamma_{d1w}(y)\gamma_{d5w}(y')\frac{\zeta_1}{H_d}(H_d/H_p)^{2\zeta_1} S_w^*(M_d, M_d'; n_1)\,dy dy' \tag{40h}$$

$$S_{Dpd111u}(n_1) = \frac{1}{4}\rho^2 b_p c_{dp} \bar{u}^2(H_d) b_d c_{dd} J_u(H_d) \int_0^{H_p}\int_{-R}^{L} \gamma_{p1u}(z)\bar{u}^2(z)J_u(z)\gamma_{d1u}(y)\left(\frac{z}{H_p}\right)^{\zeta_1}\left(\frac{H_d}{H_p}\right)^{\zeta_1} S_u^*(M_p, M_d; n_1)\,dz dy \tag{40i}$$

$$S_{Dpd115u}(n_1) = \frac{1}{4}\rho^2 \bar{u}^2(H_d) b_p b_d^2 c_{dp} c_{md} J_u(H_d) \int_0^{H_p}\int_{-R}^{L} \gamma_{p1u}(z)\bar{u}^2(z)J_u(z)\gamma_{d5u}(y)\left(\frac{z}{H_p}\right)^{\zeta_1}\frac{\zeta_1}{H_d}\left(\frac{H_d}{H_p}\right)^{\zeta_1} S_u^*(M_p, M_d; n_1)\,dz dy \tag{40j}$$

All these quantities are associated with the first mode of vibration (Fig. 6).

Finally, the nondimensional shape functions appearing in Eqs. (36) and (40) and not defined by Eq. (34) are given by:

$$\gamma_{d1w}(y) = \frac{b_d(y)}{b_d}\frac{c'_{dd}(y) - c_{ld}(y)}{c'_{dd} - c_{ld}};\ \gamma_{d5u}(y) = \frac{b_d^2(y)}{b_d^2}\frac{c_{dm}(y)}{c_{dm}};$$

$$\gamma_{d5w}(y) = \frac{b_d^2(y)}{b_d^2}\frac{c'_{dm}(y)}{c'_{dm}}\ ;\ \gamma_{d5s}(y) = \frac{b_d^2(y)}{b_d^2}\frac{c'_{msd}(y)}{c'_{msd}} \tag{41}$$

*CC*